



Microstructure and Tribological Property of TiC-Mo Composite Coating Prepared by Vacuum Plasma Spraying

Xiaoqian Guo, Yaran Niu, Liping Huang, Heng Ji, and Xuebin Zheng

(Submitted March 4, 2012; in revised form May 4, 2012)

TiC-based composite coating using Mo as an additive has been fabricated by vacuum plasma-spraying, and then the phase composition and microstructure of TiC-Mo composite coating were investigated. Wear resistance of the TiC-Mo composite coating was comparatively studied with pure TiC coating. The experimental results showed that the microstructure of the TiC-Mo composite coating was relatively homogeneous and compact, exhibiting typical lamellar structure of plasma-sprayed coating. Orientated columnar grains of TiC can be found in the composite coating, and a (Ti, Mo)C transition phase was also observed. Due to the formation of (Ti, Mo)C transition phase, strong interface between TiC and Mo splats was obtained, which positively influenced the wear performance of the composite coating. As compared with pure TiC coating, the TiC-Mo composite coating exhibited improved wear resistance both at low and high loads. Wear mechanisms for the TiC coatings have been changed by adding Mo element.

Keywords Mo, titanium carbide coating, tribological behavior, vacuum plasma spray

1. Introduction

Titanium carbide (TiC) has been a frequent choice for wear-resistant applications owing to its high hardness (Mohs 9-9.5), high melting point (3433 K), and superior chemical stability (Ref 1-3). However, the inherent brittleness of TiC restricts its wide-range applications, which makes it constantly applied as a coating onto metallic materials to utilize the mechanical strength of metals. TiC coatings/films fabricated by physical vapor deposition (PVD) and chemical vapor deposition (CVD) techniques have been studied for engineering applications since the last decade (Ref 4). PVD and CVD coatings/films are popular for their dense microstructure and good bonding to substrates; however, the low deposition rate and extremely thin thickness (normally $\leq 10 \mu\text{m}$) are unavoidable (Ref 5). Plasma-spraying technique has also drawn attention for fabricating TiC coatings (Ref 6, 7). Thick TiC coatings (thickness normally 100-1000 μm) could be successfully deposited by atmospheric plasma spraying (APS) with high deposition rate (Ref 8). However, APS technique also has its limitations. During the spraying process, plasma plume with external air could

cause serious oxidation of TiC particles, and as a result, the phase composition, microstructure, and preferred properties of TiC could be affected significantly. Vacuum plasma-spraying (VPS) process, which is carried out in controlled atmosphere, especially inert gas environment, sufficiently inhibits the oxidation of powders providing an opportunity to produce TiC coating with lower porosity, less splats oxidation, and avoidance of decomposition (Ref 9, 10).

Although VPS technique possesses some unique features to prepare hard coating materials, the deposition of refractory ceramics still exhibits some drawbacks, such as the weak intersplat cohesion (Ref 11) and the inherent undesirable defects (Ref 12). In the situation of wear-resistant applications, brittle cracks propagation could occur through these intersplats and defects, and splat or particle removal is often regarded as the primary abrasion mechanism. In order to enhance the coherence of coatings and improve their damage tolerance, metal incorporations with Ni, Fe, etc., which are usually used in TiC-based bulk materials, have been carried out to modify TiC coatings recently (Ref 13, 14). However, the limited tribological properties of these metals may depress the wear resistance of the TiC coatings. Molybdenum (Mo) is an outstanding wear-resistant metal which has been widely involved in automobile synchronizing ring or piston ring application (Ref 15). Excellent wettability to some carbides was also found for Mo, enabling it being employed to modify TiC-based composites as a wetting phase (Ref 16). Nevertheless, utilizing Mo as a toughening phase and investigating the effects of the doping of Mo on the tribological property of TiC coating are rarely reported.

In the present study, Mo was used as a second phase, aiming to improve the intersplats cohesion and subsequently enhance the wear resistance of TiC coating. VPS was applied to fabricate TiC-Mo composite coating, and

Xiaoqian Guo, Yaran Niu, Liping Huang, Heng Ji, and Xuebin Zheng, Key Laboratory of Inorganic Coating Materials, Shanghai Institute of Ceramics, Chinese Academy of Sciences, 1295 Dingxi Road, Shanghai 200050, People's Republic of China. Contact e-mails: xbzheng@mail.sic.ac.cn and naoh_gxq@126.com.

the microstructure and tribological property of the coating were characterized. The microstructural refinements and the modification of tribological behavior induced by the addition of Mo have been discussed as well.

2. Experimental Procedures

2.1 Materials

Commercially available TiC (Zhuzhou Guangyuan Cemented Material Co., Ltd, Hunan, China) and Mo (Teachn Industrial Technology Development Co., Ltd, Hunan, China) powders, with median particle sizes of 23.4 μm (D10: 7.9 μm , D50: 23.4, and D90: 49.3 μm) and 63.7 μm (D10: 44.8 μm , D50: 63.7, and D90: 85.2 μm), respectively, were used. Mixed powders consisted of 80 vol.% TiC and 20 vol.% Mo were ball milled for 8 h, and then applied for the fabrication of composite coating. Stainless steel (AISI 314) disks with dimensions of Φ 60 mm \times 8 mm were used as substrates and grit-blasted with alumina abrasive, cleaned with acetone before plasma-spraying process. Pure TiC coating was also prepared for comparison. NiCr bond coat was employed to improve the adhesion of the coatings to the substrates. The coating specimens were deposited with VPS equipment (F4-VB, Sulzer Metco, Switzerland) under the optimum parameters listed in Table 1. Argon and hydrogen were used as the plasma-forming gases. Coatings with a minimum thickness of 300 μm were prepared for wear test in this article. The mean overlapping rates for TiC and TiC-Mo coatings are 7.2 and 6.8 $\mu\text{m}/\text{pass}$, respectively.

The particle size distribution of powders was carried out by laser diffraction on BT-9300S system (Baite Instruments Ltd., China). Phase compositions of the TiC and TiC-Mo coatings were examined by an x-ray diffractometer (XRD, RAX-10, Rigaku, Japan) operating with Cu K_{α} ($\lambda=1.54056 \text{ \AA}$) radiation. Surface morphologies and cross sections of the coatings were observed using a scanning electron microscope (SEM, JSM-6700, JEOL, Japan) equipped with an energy dispersive spectroscope (EDS). The cross-sectional SEM images were employed for porosity measurement using image software (Qwin, Leica, Germany). The HX1000 microindenter (Shanghai Taiming Optical Instrument Co., Ltd., China) was employed to measure Vickers microhardness on polished cross sections. Microstructures of the coatings were

Table 1 Plasma-spraying operating parameters

Parameters	TiC based coatings	Bond coat
Chamber pressure, mbar	300	100
Spray distance, mm	260	320
Powder, kW	41	33
Primary gas/Ar, slpm	50	35
Secondary gas/H ₂ , slpm	10	8
powder feed speed, g/min	22	30
Carrier gas type and flow, slpm	Ar, 3	Ar, 3
Spray gun scanning rate, m/s	400	400

characterized with a transmission electron microscope (TEM, JEM-200CX, JEOL, Japan).

2.2 Wear Test

Wear tests were performed on a multifunctional tribometer (UMT-2, CETR, USA) using ball-on-disk contact configuration. The schematic diagram of the wear tester is shown in Fig. 1. The coating specimen was fixed on a rotating disk using a screw in the center of the sample, while WC-Co with hardness of HRC 92 was used as the ball (9.2 mm in diameter) specimen. The tribological samples were polished to $R_a=0.2$ using diamond abrasive paste. The wear tests were carried out at room temperature with a relative humidity of about 30%. The total sliding time was 30 min with sliding speed of 0.5 m/s. The normal loads applied were 20 and 50 N. Friction coefficients were online monitored, and wear rates of the coating were determined as follows:

$$W = \frac{V}{F \cdot vt} \quad (\text{Eq 1})$$

$$V = 2\pi R \cdot S \quad (\text{Eq 2})$$

where W ($\text{mm}^3/\text{N}\cdot\text{m}$) is the wear rate, V (mm^3) is the wear volumes, F (N) is the applied load, v (m/s) and t (s) stand for sliding speed and sliding time, respectively, R (mm) is the rotation radius of the counter-ball, S (mm^2) is the area of the wear track's cross section which is measured by a profilometer (T8000-C, Hommelwerke, Germany). Five tests were repeated for each experimental condition. Wear tracks of the samples were examined using SEM and EDS.

3. Results and Discussion

3.1 Microstructure Characteristics

XRD patterns of the TiC and TiC-Mo composite coatings are shown in Fig. 2. It can be seen that both the TiC and TiC-Mo coatings crystallized well, and the

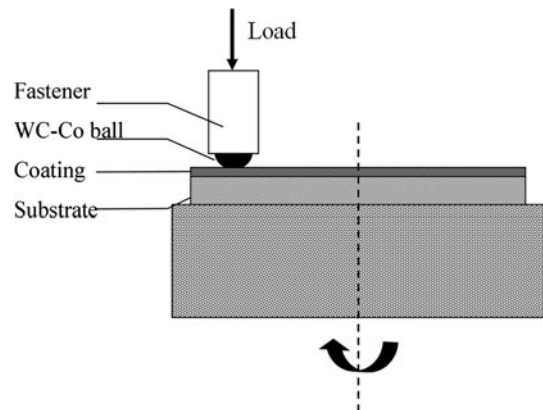


Fig. 1 Schematic diagram of the ball-on-disk friction and wear test apparatus

composite coating consisted mainly of face-centered cubic (fcc) TiC phase and body-centered cubic (bcc) Mo phase. Besides, according to the JCPDS cards, some non-stoichiometric carbides such as $\text{TiC}_{0.981}$ and $\text{Ti}_{0.98}\text{C}$ are probably also formed in the as-sprayed coatings due to splat quenching. Evidence of titanium oxide phase, which was usually found in APS-TiC coatings (Ref 7), was not

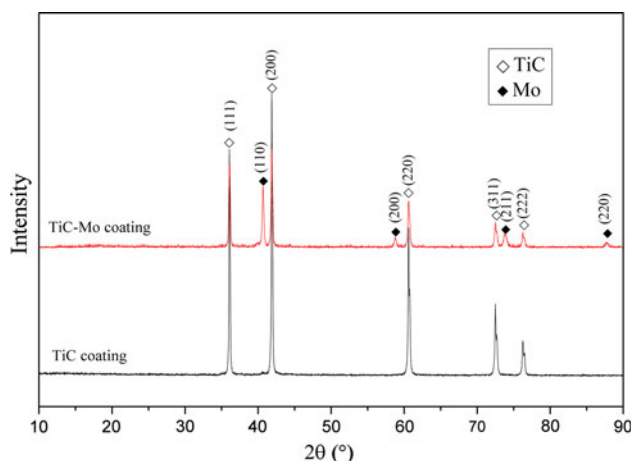


Fig. 2 XRD patterns of TiC and TiC-Mo composite coatings

detected in this investigation, indicating that the protective environment of VPS process effectively inhibited the formation of titanium oxides.

SEM micrographs in Fig. 3 display the surface and cross-sectional morphologies of TiC and TiC-Mo composite coatings. The TiC coating exhibited loose and poorly consolidated surface (Fig. 3a), cross section of which was pervaded with spherical and ellipsoidal pores produced by stacking of unmelted splats (Fig. 3b). The overall porosity determined by the image analysis was about $(8.6 \pm 0.7)\%$. Differing from the pure TiC coating, the TiC-Mo composite coating exhibited denser and typical lamellar microstructure (Fig. 3d), where Mo (pale region, confirmed by EDS) distributed homogeneously in TiC phase (dark region). Although the localized defects such as pores, unmelted particles, still can be found in the TiC-Mo coating, the average porosity of the coating has dropped to $(4.8 \pm 1.2)\%$. This could be attributed to the efficient spreading, overlapping and filling of Mo droplets in the coating. As displayed in Fig. 3(c), some fully melted Mo particles were well flattened, producing smoother surface for the composite coating. One should mention that, even though TiC-Mo coatings exhibit quite different microstructure and porosity value, the corresponding microhardness values obtained for TiC-Mo composite coatings ($621 \pm 86 \text{ HV}_{0.05}$) are similar to those of pure

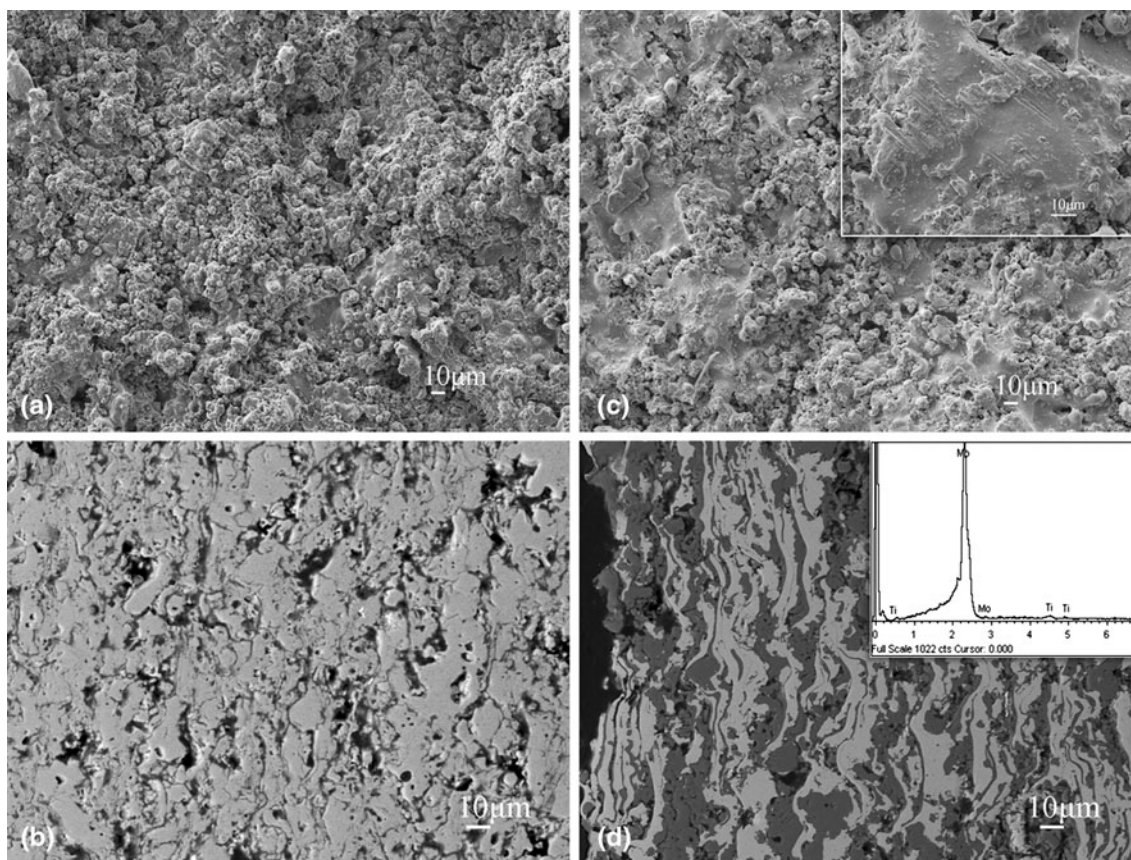


Fig. 3 SEM micrographs of TiC and TiC-Mo composite coating: (a) and (b) TiC coating, (c) and (d) TiC-Mo composite coating

TiC coatings ($616 \pm 58 \text{ HV}_{0.05}$), and the difference in hardness values is less than 5%.

TEM observation has been conducted on both transverse and longitudinal sections of the TiC-Mo composite coating. Figure 4 presents the microstructure of the transverse section (perpendicular to the spraying direction) of the TiC-Mo composite coating. It can be observed that the composite coating possessed complex polycrystalline structure, which can be divided into three different crystallizing regions. One is the perfect crystallization region (A) consisting of equiaxed and regular nanoscale TiC grains with an average grain size of about 50-100 nm, where typical intergranular fracture can also be found (Fig. 4b). The region (B), which consisted of lots of *large grains* approximately of size, 150 nm, confirmed to be Mo by EDS, was also found in the TEM observation (Fig. 4c). The third region (C) was transition region between (A)

and (B), consisting of elements of Ti and Mo. The formation of (Ti, Mo)C transition phase (Ref 16) could be attributed to the interdiffusion between TiC and Mo during discontinuous solidification. This (Ti, Mo)C phase is quite similar with the *Mo-rich shell* in sintered materials which could improve the wettability between ceramic and metallic phases (Ref 17, 18). Based on the fact that TiC belongs to the group IV transition metal carbides in which the octahedral interstitial sites of metallic fcc sub-lattice may be partially filled with carbon atoms, Mo could diffuse into TiC phase, fill the structural vacancy of TiC, and consequently form a *Mo-rich shell* at the contact points between particles (Ref 19).

The TEM images of the longitudinal section of TiC-Mo composite coating are shown in Fig. 5. It can be found that the coatings were built up from splats overlapping each other, and most of these splats exhibited similar

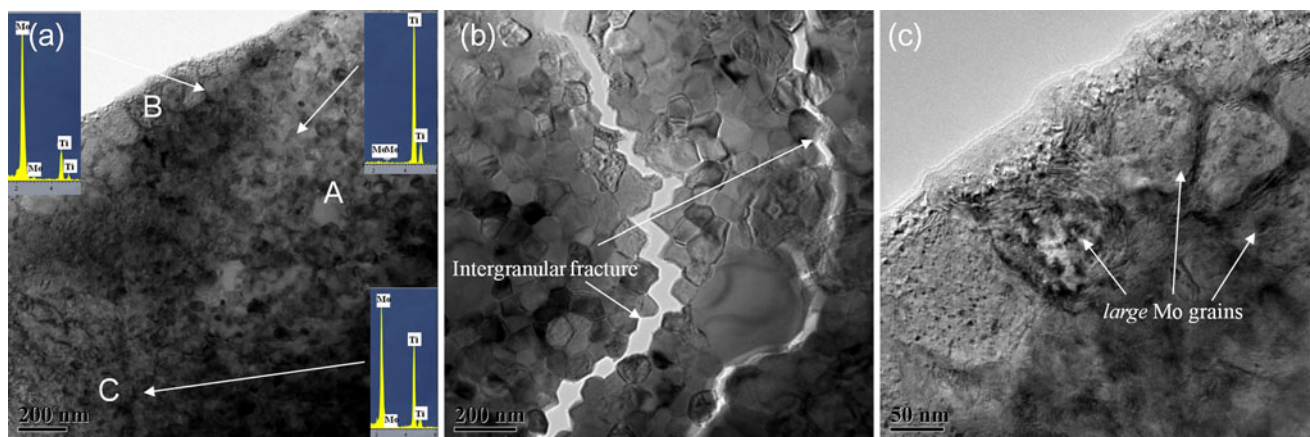


Fig. 4 TEM micrographs obtained from transverse section of the TiC-Mo composite coating: (a) overall crystallization morphology, (b) region with regular nanoscale grains, and (c) region with *large grains*

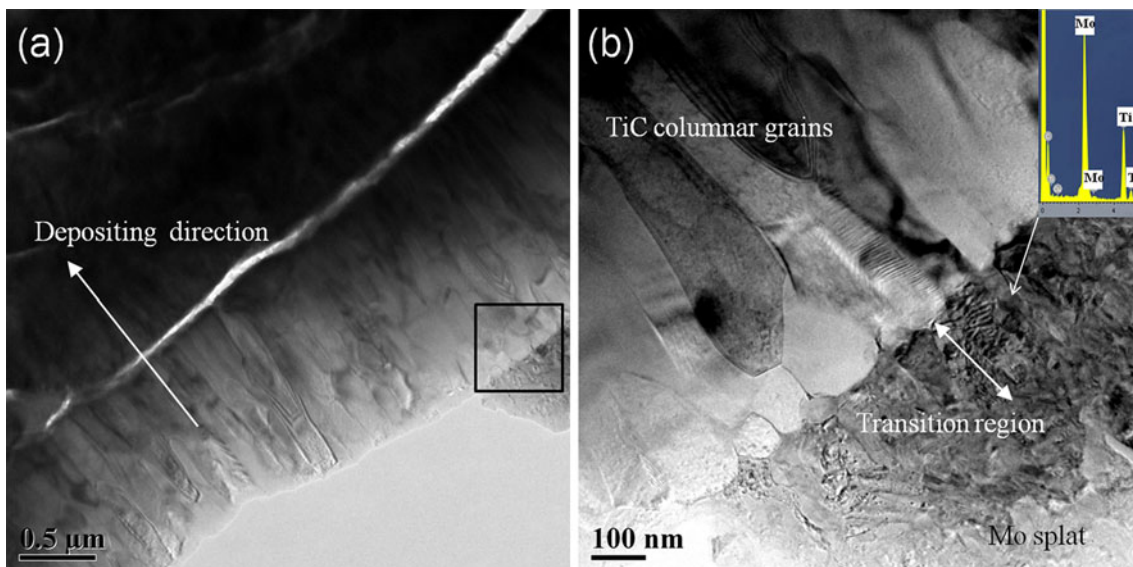


Fig. 5 TEM micrographs obtained from longitudinal section of the TiC-Mo composite coating: (a) lamellar structure and (b) TiC/ Mo intersplat

characteristics of parallel columnar grains diameters of which were approximately 100 nm (Fig. 5a). EDS analysis verified these directional arranged columnar grains to be TiC. Detailed information suggested that the columnar grains oriented along the direction of the heat flow released. The droplet spread out, and the heat was transported away as soon as it hit the underlying material. Then, solidification commenced heterogeneously at the interface between the splat and underlying material. Grains nucleated and rapidly grew into the molten splat, forming a columnar grain structure (Ref 20). Delaminations were visible at the interface between the splats composed of regular columnar grains (Fig. 5a), illustrating a weak cohesion between TiC splats. The interface between TiC and Mo splats, however, exhibited a well-developed bond owing to the formation of a transition phase, as shown in Fig. 5(b). The longitudinal morphologies of TiC-Mo coating actually are quite consistent with the transverse morphologies shown in Fig. 4. The orientated TiC columnar grains, Mo splat, and (Ti, Mo)C transition phase, shown in Fig. 5(b), respectively, correspond to the regions A, B, and C in Fig. 4.

Distinct morphologies of the interfaces between TiC splats are shown in Fig. 6. As can be seen, only a few of these interfaces exhibited continuity, even through the TiC splats were completely melted. Spherical and ellipsoidal pores can be easily distinguished at the interfaces of the well-melted TiC splats (Fig. 6a). Long ellipsoidal pores also can be found at the interface between well-melted and unmelted TiC splats (Fig. 6b). This weak adhesion was believed to arise from splats stacking faults, gas entrapments, or the mismatching of the interfaces resulted from the discontinuous solidification in the process of plasma spraying. This brings us to an unfortunate possibility that, if cyclic shear force acts on the TiC brittle phase during wear process, it would lead to crack initiation and propagation, and material peeling off in the result (Ref 21). It is gratifying to note that owing to the formation of (Ti, Mo)C transition phase in the TiC-Mo composite coating, the interfaces between TiC and Mo splats have been significantly enhanced.

3.2 Tribological Properties

Wear test results of the TiC and TiC-Mo composite coatings at low and high loads were summarized and compared in Fig. 7. As can be seen, the TiC-Mo composite coatings underwent much less material loss and displayed relatively low friction coefficient on both low- and high-load conditions. Especially under the lower-load condition (20 N), the wear rate of the TiC-Mo coating was only a half of pure TiC coating, exhibiting superior wear performance. Under the test condition of 50 N and 0.5 m/s, even through the friction coefficient of composite coating was quite similar with that of pure TiC coating, the composite coating exhibited a lower wear rate.

Figure 8 shows the corresponding worn surfaces of TiC and TiC-Mo composite coating at the applied load of 50 N, sliding speed of 0.5 m/s. Localized delaminations, flaking pits, as well as slight scratches can be found on the worn surfaces of the pure TiC coating (Fig. 8a and 8b),

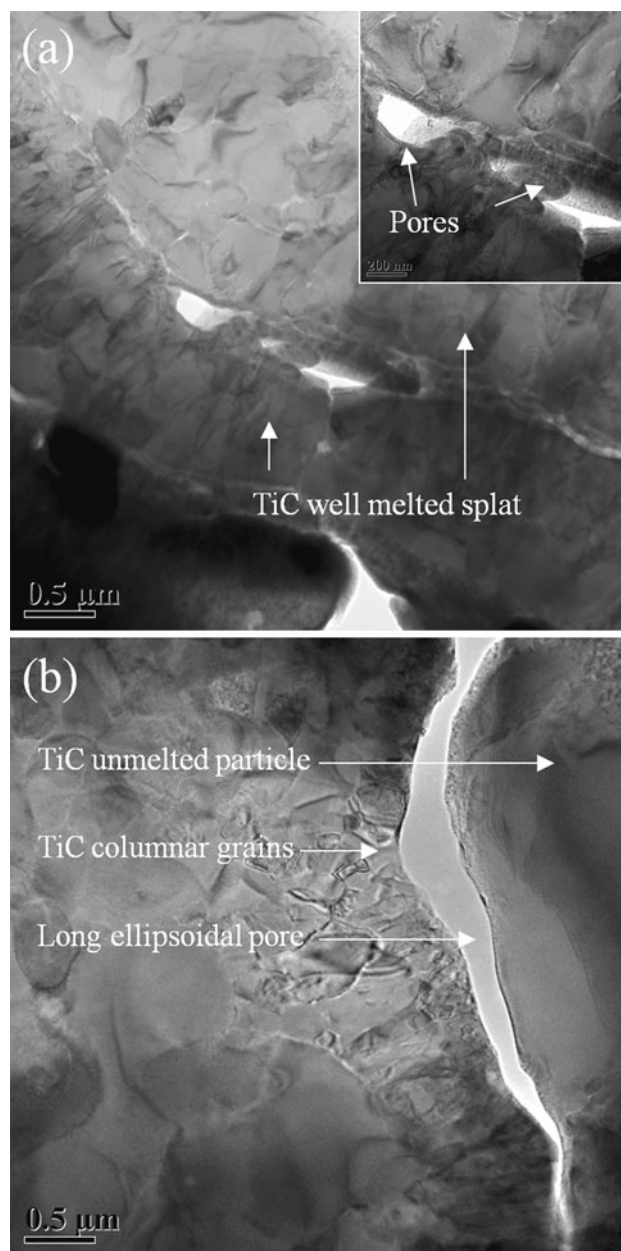


Fig. 6 TEM micrographs of the interface: (a) interface between TiC splats and (b) interface between TiC columnar grains and TiC unmelted particles

indicating that the predominant wear mechanisms were particle pull out and fatigue flake off. The corresponding cross-sectional profiles inserted in Fig. 8(a) suggested that the wear track was over 600 μm in width. The wear tracks of the TiC-Mo composite coating shown in Fig. 8(c) and 8(d) revealed that the composite coatings experienced more moderate wear loss compared with pure TiC coatings. It is obvious that the surface of TiC-Mo composite coating was much smoother than that of the pure TiC coating (Fig. 8c). Despite the appearance of some ploughing grooves parallel to sliding direction as indicated in Fig. 8(c) and 8(d), the wear tracks rims in the TiC-Mo

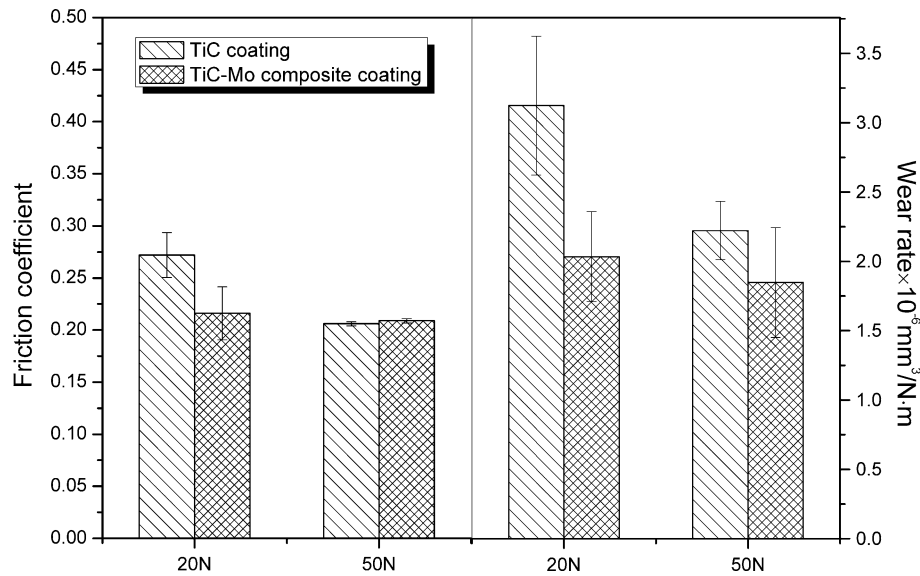


Fig. 7 Comparison of tribological behaviors between TiC and TiC-Mo composite coatings at sliding speed of 0.5 m/s

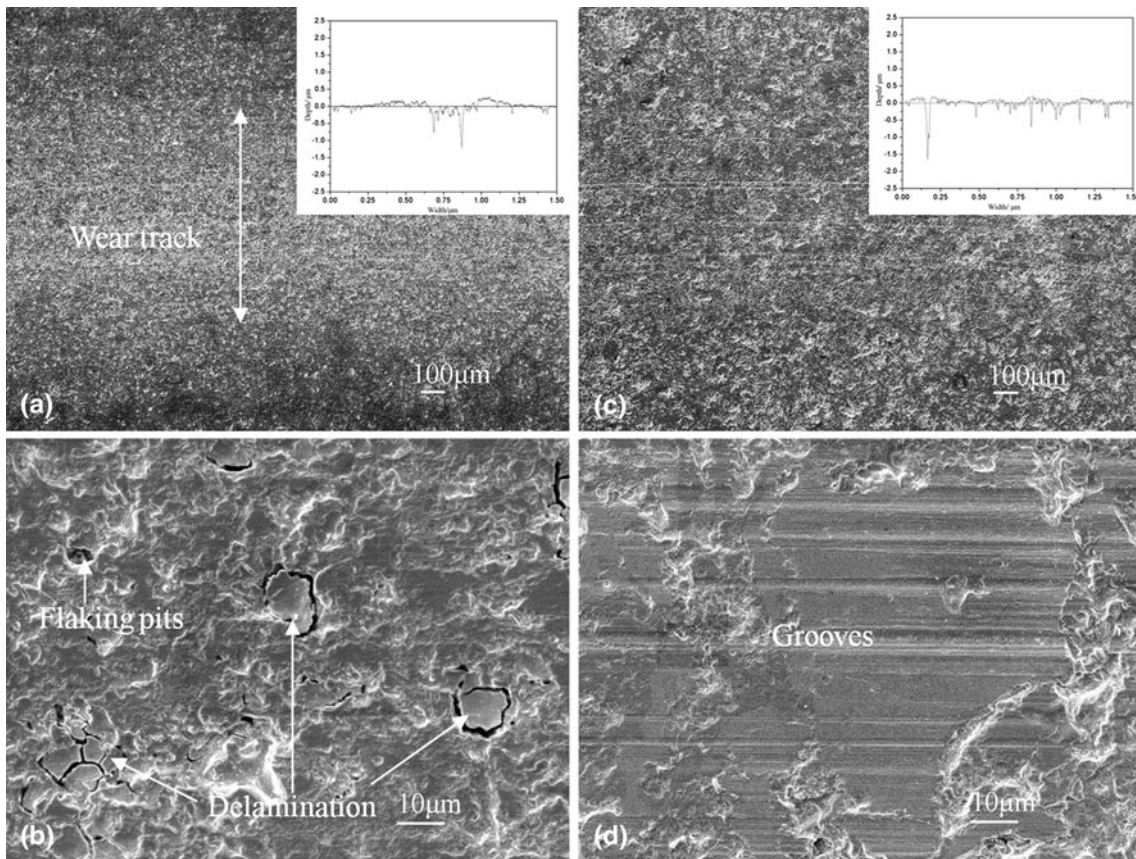
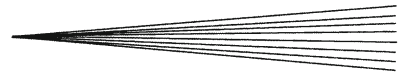


Fig. 8 SEM micrographs of wear track after 1800-s sliding against WC-Co ball with the applied load 50 N, sliding speed, 0.5 m/s: (a) and (b) TiC; (c) and (d) TiC-Mo

coating were nearly undistinguishable compared with those of the TiC coating. This also can be verified through the worn profile analysis inserted in Fig. 8(c). The broader and shallower worn profile of the TiC-Mo coating

indicated that plastic deformation happened during the wear test, which alleviated the effect of stress concentration to some degree (Ref 22). Wear damages of these composite coatings were restrained to some grooves



resulted from extruding and ploughing. Little delaminations were found in the wear tracks of the composite coating, which was quite different from the pure TiC coating.

From the results obtained, it is supposed that the possible cracking in TiC coating can be divided into three categories: (1) cracking around the unmelted particles. This situation almost certainly exists because of the high melting point of TiC; (2) cracking at the interfaces between splats parallel to the substrate, which can be attributed to the weak cohesion of the splats; (3) cracking along the columnar grain boundaries (just like Fig. 4b) (Ref 23-25). Actually, these possible crack initiation regions usually endure discontinuous strain or compressive stress during wear tests (Ref 26, 27). Once the stress exceeds the fatigue limit of the material during the cyclic contact process, cracks would be nucleated and propagated. Thus, particle pull out and fatigue flake off will take place in these sites. The TiC-Mo composite coatings exhibited a good splat adhesion due to the formation of (Ti, Mo)C transition phase, which prevented the well-adhered splats to crack along the interface of the splats. The perfect ductility of Mo can also effectively release the stress concentration experienced during wear tests (Ref 28), which improves significantly the wear resistance of the TiC-Mo composite coatings.

4. Conclusions

TiC-Mo composite coating was fabricated by VPS technique successfully, and the microstructures as well as tribological properties of the TiC-Mo were investigated. It is found that the composite coating was mainly composed of TiC (fcc) and Mo (bcc) phases. The protective environment of VPS process efficiently inhibited the formation of titanium oxides. Lamellar microstructure was found for the TiC-Mo composite coating, porosity of which (4.8 ± 1.2)% was much lower than that of pure TiC coating (8.6 ± 0.7)%. A (Ti, Mo)C transition phase between TiC parallel columnar grains and Mo splats was found. Improved interface owing to the formation of this (Ti, Mo)C phase influenced positively the wear performance of the composite coating. The TiC-Mo composite coating exhibited outstanding wear resistance both at low and high loads, and the main wear mechanism of the coating was confirmed to be that of ploughing.

Acknowledgments

This study was jointly supported by the National Natural Science Foundation (for Young Scholar) of China under grant 51102267, Shanghai Science and Technology R&D Fund under grant 11ZR1442100.

References

1. A. Schroer, H. Boving, and F. Fluhmann, TiC-Coated Balls for Special Bearings, *Vak. Forsch. Prax.*, 2000, **2**, p 114-116
2. L.R. Katipelli, A. Agarwal, and N.B. Dahotre, Laser Surface Engineered TiC Coating on 6061 Al Alloy: Microstructure and Wear, *Appl. Surf. Sci.*, 2000, **153**, p 65-78
3. X. Zhang, J. Ma, J. Yang, Q. Bi, and W. Liu, Dry-Sliding Tribological Behavior of Fe-28Al-5Cr/TiC Composites, *Wear*, 2011, **277**, p 881-888
4. A. Teber, F. Schoenstein, F. Tetard, M. Abdellaoui, and N. Jouini, Effect of SPS Process Sintering on the Microstructure and Mechanical Properties of Nanocrystalline TiC for Tools Application, *Int. J. Refract. Met. Hard Mater.*, 2012, **30**(1), p 64-70
5. G. Bolelli, J. Rauch, V. Cannillo, A. Killinger, L. Lusvarghi, and R. Gadow, Microstructural and Tribological Investigation of High-Velocity Suspension Flame Sprayed (HVSFA) Al₂O₃ Coatings, *J. Therm. Spray Technol.*, 2009, **18**(1), p 35-49
6. S. Economou and M. De Bone, Tribological Behaviour at Room Temperature and at 550°C of TiC-Based Plasma Sprayed Coatings in Fretting Gross Slip Conditions, *Wear*, 2000, **244**(1-2), p 165-179
7. H.-D. Steffens, M. Dvorak, and P. Groot, Thermal Behaviour of Thick TiC Layers Made by Plasma Spraying, *Surf. Coat. Technol.*, 1991, **49**, p 46-49
8. Y. Niu, Microstructure and Properties Characterization of Silicon Coatings Prepared by Vacuum Plasma Spraying Technology, *J. Therm. Spray Technol.*, 2009, **18**(3), p 427-434
9. Y. Niu, X. Zheng, H. Ji, and L. Qi, Microstructure and Thermal Property of Tungsten Coatings Prepared by Vacuum Plasma Spraying Technology, *Fusion Eng. Des.*, 2010, **85**, p 1521-1526
10. G. Bolelli, L. Lusvarghi, T. Manfredini, and F. Pighetti Mantini, Comparison Between Plasma- and HVOF-Sprayed Ceramic Coatings. Part I: Microstructure and Mechanical Properties, *Int. J. Surf. Sci. Eng.*, 2007, **1**(1), p 38-60
11. X. Qi, E. Aust, N. Eigen, F. Fartner, and R. Bormann, Abrasive Wear Mechanisms of VPS- and HVOF-Sprayed TiC-Ni Based Nanocrystalline Coatings, *Mat.-wiss. u. Werkstofftech.*, 2004, **35**, p 779-784
12. M. Le Flem, A. Allemand, S. Urvoy, D. Cédât, and C. Rey, Microstructure and Thermal Conductivity of Mo-TiC Cermets Processed by Hot Isostatic Pressing, *J. Nucl. Mater.*, 2008, **380**, p 85-92
13. J. Xu, W. Liu, and M. Zhong, Microstructure and Dry Sliding Wear Behavior of MoS₂/TiC/Ni Composite Coatings Prepared by Laser Cladding, *Surf. Coat. Technol.*, 2006, **200**, p 4227-4232
14. J. Liu, TiC/Fe Cermets Coating by Plasma Cladding Using Asphalt as a Carbonaceous Precursor, *Prog. Nat. Sci.*, 2008, **18**, p 447-454
15. B. Hwang, S. Lee, and J. Ahn, Correlation of Microstructure and Wear Resistance of Molybdenum Blend Coatings Fabricated by Atmospheric Plasma Spraying, *Mater. Sci. Eng. A*, 2004, **366**, p 152-163
16. Q. Wu, C. Yang, F. Xue, and Y. Sun, Effect of Mo Addition on the Microstructure and Wear Resistance of In Situ TiC/Al Composite, *Mater. Des.*, 2011, **32**, p 4999-5003
17. Y. Li, N. Liu, X. Zhang, and C. Ron, Effect of Mo Addition on the Microstructure and Mechanical Properties of Ultra-Fine Grade TiC-TiN-WC-Mo₂C-Co Cermets, *Int. J. Refract. Met. Hard Mater.*, 2008, **26**, p 190-196
18. T. Chraska and A.H. King, Transmission Electron Microscopy Study of Rapid Solidification of Plasma Sprayed Zirconia—Part II: Interfaces and Subsequent Splat Solidification, *Thin Solid Films*, 2001, **397**, p 40-48
19. D. Cédât, C. Rey, M. Clavel, J.H. Schmitt, M. Le Flem, and A. Allemand, Microstructural Characterization of a Composite Mo Reinforced by 25 at.% TiC, *J. Nucl. Mater.*, 2009, **385**, p 533-537
20. P. Bengtsson and T. Johannesson, Characterization of Microstructural Defects in Plasma-Sprayed Thermal Barrier Coatings, *J. Therm. Spray Technol.*, 1995, **4**(3), p 245-251
21. J.M. Guilemany, S. Armada, and J.M. Miguel, Evaluation of Wear Damage in Zirconia Plasma-Sprayed Coatings Using Scanning White Light Interferometry, *J. Therm. Spray Technol.*, 2001, **10**(1), p 142-146
22. Y. Xie and H.M. Hawthorne, The Damage Mechanisms of Several Plasma-Sprayed Ceramic Coatings in Controlled Scratching, *Wear*, 1999, **233-235**, p 293-305

23. X. Zhang, J. Ma, Q. Bi, and W. Liu, Dry-Sliding Tribological Behavior of Fe-28Al-5Cr/TiC Composites, *Wear*, 2011, **271**, p 881-888
24. T. Chraska and A.H. King, Effect of Different Substrate Conditions upon Interface with Plasma Sprayed Zirconia-a TEM Study, *Surf. Coat. Technol.*, 2002, **157**, p 238-246
25. Q. Luo, W.M. Rainforth, and W.-D. Münz, TEM Observations of Wear Mechanisms of TiAlCrN and TiAlN/CrN Coatings Grown by Combined Steered-Arc/Unbalanced Magnetron Deposition, *Wear*, 1999, **225-229**, p 74-82
26. B. Uyulgan, H. Cetinel, I. Ozdemir, C. Tekmen, S.C. Okumus, and E. Celik, Friction and Wear Properties of Mo Coatings on Cast-Iron Substrates, *Surf. Coat. Technol.*, 2003, **174-175**, p 1082-1088
27. G. Bolelli, V. Cannillo, L. Lusvarghi, and T. Manfredini, Wear Behavior of Thermally Sprayed Ceramic Oxide Coatings, *Wear*, 2006, **261**, p 1298-1315
28. T. Polocar, T. Kubart, R. Novák, L. Kopecký, and P. Šíroký, Comparison of Tribological Behavior of TiN, TiCN and CrN at Elevated Temperatures, *Surf. Coat. Technol.*, 2005, **193**, p 192-199